

- [4] A. Thess, R. Lee, P. Nikolaev, H. Dai, P. Petit, J. Robert, C. Xu, Y. H. Lee, S. G. Kim, D. T. Colbert, G. Scuseria, D. Tománek, J. E. Fisher, R. E. Smalley, *Science* **1996**, 273, 483.
- [5] Y. H. Lee, S. G. Kim, D. Tománek, *Phys. Rev. Lett.* **1997**, 78, 2393.
- [6] C. Journet, W. K. Maser, P. Bernier, A. Loiseau, M. Lamy de la Chapelle, S. Lefrant, P. Deniard, R. Lee, J. E. Fischer, *Nature* **1997**, 388, 756.
- [7] H. Dai, E. W. Wang, Y. Z. Lu, S. Fan, C. Lieber, *Nature* **1995**, 375, 769.
- [8] W. Han, S. Fan, Q. Li, Y. Hu, *Science* **1997**, 277, 1287.
- [9] J. Zhu, S. Fan, *J. Mater. Res.* **1999**, 14, 1175.
- [10] S. T. Lee, N. Wang, Y. F. Zhang, Y. H. Tang, *MRS Bull.* **1999**, 24, 36.
- [11] Yttrium powder in spindle oil was originally purchased from High Purity Chemicals. Oil was repeatedly evaporated in *n*-hexane solution. Purified yttrium was further mixed with Ni and Co powders (2 N, High Purity Chemicals) with an appropriate weight ratio.
- [12] Y. C. Choi, Y. H. Lee, unpublished.
- [13] J.-M. Bonard, T. Stora, J.-P. Salvetat, F. Maier, T. Stockli, C. Daschl, L. Forro, W. A. de Heer, A. Chatelain, *Adv. Mater.* **1997**, 9, 827.
- [14] H. Hiura, T. W. Ebbesen, K. Tanigaki, *Adv. Mater.* **1995**, 7, 275.
- [15] We also observed nanowires with amorphous surface layers, where no transition metals were found on the surface and, in particular, no twin defects were observed in such nanowires.
- [16] C. W. Oh, E. Kim, Y. H. Lee, *Phys. Rev. Lett.* **1996**, 76, 776.
- [17] JCPDS card no. 43-1012.
- [18] H. Z. Zhang, Y. C. Kong, Y. Z. Wang, X. Du, Z. G. Bai, J. J. Wang, D. P. Yu, Y. Ding, Q. L. Hang, S. Q. Feng, *Solid State Commun.* **1999**, 109, 677.
- [19] The characteristic X-rays for EDXRS analysis were accumulated for 100 s with an ultra-thin window type detector at an accelerating voltage of 300 keV, which enabled us to detect the  $K\alpha$  peak of O at 0.52 keV.
- [20] L. C. Qin, D. Zhou, A. R. Krauss, D. M. Gruen, *Appl. Phys. Lett.* **1998**, 72, 3437.
- [21] We observed through the window that bluish gases were formed during the reaction, suggesting the formation of  $\text{NO}_x$  gas. This excludes the possibility of forming  $\text{N}_2$  gas.
- [22] *HSC Chemistry*, ver. 3.0, Outokumpu Research Oy, Pori, Finland **1997**.
- [23] The standard Gibbs free energy varies with temperature. This value becomes maximum ( $\sim 570$  kJ/mol) at 2300 K and decreases with increasing temperature. The reaction temperature in arc discharge is usually greater than 5000 K, again ensuring a more preferable reaction occurs.
- [24] R. L. Schwoebel, *J. Appl. Phys.* **1969**, 40, 614.

## Single-Walled Carbon Nanotube–Polymer Composites: Strength and Weakness\*\*

By Pulickel M. Ajayan,\* Linda S. Schadler, Cindy Giannaris, and Angel Rubio

Carbon nanotubes are near ideal whiskers consisting of folded graphene layers with cylindrical hexagonal lattice structure. During growth, depending on the conditions in which they are formed, they assemble either as multiwalled co-axial tubules (multiwalled nanotubes, MWNTs) or as

bundles (ropes) consisting of individual cylinders (single-walled nanotubes, SWNTs) packed in two-dimensional triangular lattices. Recent experimental studies<sup>[1]</sup> and theoretical modeling<sup>[2]</sup> have amply demonstrated that individual nanotubes have extremely high Young's modulus ( $\sim 1.2$  TPa), stiffness and flexibility. Their application as structural reinforcement, however, (specifically in polymer composites) is going to depend on the ability to transfer load from the matrix to the nanotubes.<sup>[3]</sup>

The techniques used to understand the load transfer and the failure of nanotubes have been micro-Raman spectroscopy<sup>[4]</sup> and a Kelly–Tyson approach to measuring the interfacial shear stress.<sup>[5]</sup> These studies have given some evidence for good load transfer between the polymer and the nanotubes. The Kelly–Tyson approach requires fragmenting the nanotubes, but it is unclear if the failures observed in the MWNT and SWNT composites are failures of individual tubes or local instabilities of the aggregates (MWNT or SWNT bundles). Clearly for SWNTs, the failure could result either from nanotubes pulling out of bundles or from the actual fracture of individual nanotubes in the bundles.

Micro-Raman spectroscopy can also be used to understand load transfer in MWNTs because the second-order  $A_{1g}$  (disorder-induced) Raman peak position shifts with applied strain. If the nanotubes are carrying strain, then the Raman peak will have a large shift with applied composite strain. Lourie and co-workers observed a  $6\text{ cm}^{-1}$  shift in MWNTs under hydrostatic compression using thermal loading,<sup>[4]</sup> and even larger shifts for SWNT samples.<sup>[6]</sup> Schadler et al.<sup>[7]</sup> observed a  $6\text{ cm}^{-1}$  shift in MWNTs in compression and no shift in tension, implying that load transfer in tension to the MWNTs was negligible. This was attributed to the fact that the inner tubes were sliding within the outer tubes and hence the load was not effectively transmitted to all the layers in the coaxial MWNT assembly, or due to possible extremely low interfacial shear stresses between the tubes and the matrix arising from poor interfacial bonding. This mechanism of deformation has been confirmed by pulling individual MWNTs to failure using two atomic force microscopy (AFM) tips.<sup>[8]</sup>

In SWNTs the second-order  $A_{1g}$  mode has been monitored as a function of applied composite strain. Lourie and co-workers observed a 21 wavenumber shift per percentage strain in SWNT composites using thermal loading.<sup>[4]</sup> More recent work by Wood et al. has shown significant Raman shifts for SWNTs in hydrostatic compression using a diamond anvil cell.<sup>[6]</sup> It is unclear, however, if this shift indicates radial strain on individual SWNTs; it is more likely that a shift in this mode indicates radial strain in the nanotube bundles.

Our experiments here deal with observations of local elastic behavior of individual single-walled nanotube bundles and load transfer in epoxy composites as well as pressed pellets of composites containing SWNTs and carbonaceous soot material formed during nanotube synthesis. The fabrication of the epoxy SWNT composite (5 wt.-%

[\*] Prof. P. M. Ajayan, Prof. L. S. Schadler, C. Giannaris  
Department of Materials Science and Engineering  
Rensselaer Polytechnic Institute  
Troy, NY 12180-3590 (USA)  
Dr. A. Rubio  
Departamento de Física Teórica  
Universidad de Valladolid  
E-47011 Valladolid (Spain)

[\*\*] The work was supported by the DMR division of the National Science Foundation for work on carbon nanotubes through the CAREER grant, the European Community TMR program under contract ERBFMRX-CT96-0067 (DG12-MIHT), and JCYL (Grant: VA28/99).

nanotubes) followed the same procedure used in the case of MWNTs, as reported earlier.<sup>[7]</sup> The composites were loaded axially in tension and compression and the second-order  $A_{1g}$  mode was observed using Raman spectroscopy as a function of applied strain. An excitation frequency of 514.5 nm and a back-scattering geometry was used to collect the Raman spectra. After failure, the fracture surface was examined in detail using scanning electron microscopy (SEM). To form the carbon-carbon composite pellets, the sample of nanotubes formed in the electric arc (using a Ni-Y catalyst) was acid treated to dissolve the metal particles, filtered through 1  $\mu\text{m}$  pore size polycarbonate membranes to remove large aggregates of disordered and glassy carbon, dried, and pressed. Microcracks of varying widths, formed in the pellets, were examined by SEM to observe the configurations of nanotubes that bridge these cracks.

Two striking observations were seen in the epoxy composites on the application of stress and after composite fracture took place. A typical fracture surface consisted of a network of SWNT bundles that cover the surface (Fig. 1a). From the morphology of the nanotube network, it looks as if the tube bundles have been pulled out of the matrix during the deformation and fracture of the composites; these pulled out bundles have fallen back onto the broken surfaces as a loose network. This can be contrasted from other areas of the fracture surface where the nanotubes are not entirely pulled out but fully stretched (Fig. 1b). It seems

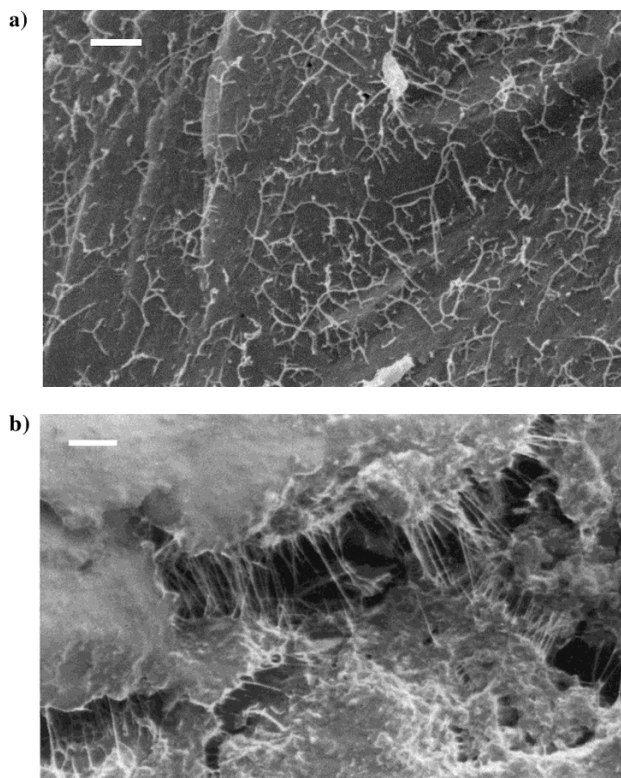


Fig. 1. a) SEM micrograph showing a network of SWNT aggregates collapsed on the surface of a fractured nanotube-epoxy composite. b) SEM micrograph of SWNT bundles stretched across a crack opening in a nanotube-epoxy composite. Scale bars in the images correspond to 1  $\mu\text{m}$ .

here that the local deformation was not enough to pull out nanotubes from the tube bundles. The stretched nanotube bundles are well aligned. This is clear indication that stretching can align nanotube bundles easily, as reported in earlier works.<sup>[9]</sup>

The case of the nanotube-reinforced pellet provides a clearer picture of what is happening. We examined cracks of several widths, from a few tens of nanometers to several micrometers. The configuration of nanotubes across these cracks follows three typical patterns depending on the ratio ( $L/d$ ) between average nanotube length  $L$  (of the order of micrometers) and separation  $d$  between the surfaces of the crack. If the width of the crack was large (typically,  $>3 \mu\text{m}$  with  $L/d < 1$ ), no nanotubes were observed in the region between the crack faces. This is the case where all the nanotube bundles have been completely pulled out from the separating broken fragments; the morphology of the fracture surface here should be similar to what was observed in Figure 1a. When the crack separation is of intermediate length (close to a micrometer or so) we observed well-aligned and stretched nanotube bundles bridging the cracks (Fig. 2a). The situation is similar to that seen in Figure 1b where the nanotubes have been pulled but not to the extent where pullout of individual tubes out of the bundles breaks the bundles. In the third case, when the crack width is sev-

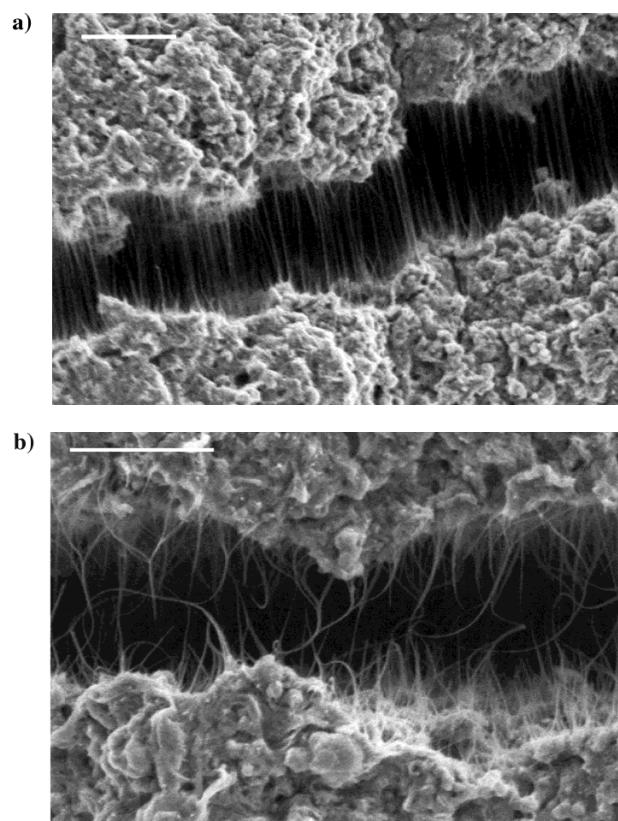


Fig. 2. a) SEM micrograph of SWNT bundles stretched across cracks observed in a nanotube-carbon composite pellet for certain critical crack widths. b) Curved bundles of SWNT that are no longer under load, as observed in an SEM image. The scale bars in the images correspond to 1  $\mu\text{m}$ .

eral tens to a few hundred nanometers, most nanotubes are curved and looped (Fig. 2b); few are seen stretched since the crack separation is not uniform. This is due to the fact that typically during fracture, the crack opens, stretches the reinforcing nanotubes, and subsequently closes somewhat (relaxes), removing the load on the nanotubes.

The curving and stretching emphasizes the high flexibility of the nanotube bundles experienced over localized areas of the composite and their ability to damp the applied deformation. This behavior might be of importance in increasing the toughness of the composite because the nanotubes could pull out from many directions without failing. This would increase the effectiveness of the pullout and crack bridging contributions to toughness. Similarly, the pullout lengths of the tubes from bundles could be long depending on the lengths of individual tubes in the bundle (terminated at different lengths inside the bundle structure) and would involve continuous absorption of energy in overcoming the van der Waals attraction between adjacent tubes. This modular elongation behavior (occurring as different stages in the pullout) can be compared to the elongation events that occur in naturally occurring composites such as nacre where the adhesive polymer chains elongate discontinuously, resulting in energy absorption and increased fracture toughness.<sup>[10]</sup> The structure of the nanotube bundle, which is easily twisted, buckled, and entangled, can be seen as a particular case of a fiber that can be continuously and, in a stepwise manner, modulated. Such modulation will allow the release of stresses in the composite without breaking, and will provide toughness to the composite (see Figs. 2a and 2b for the transition between entangled and straight-aligned tubes).

In order to take advantage of the high Young's modulus of SWNTs in polymer composites, load must be transferred from the matrix to the nanotubes. We hypothesize that the load transfer to the nanotubes is limited because the nanotubes are slipping within the bundles. In addition, the failure we observe at large crack distances is not failure of individual tubes, but the bundles falling apart. We shall further discuss this scenario. First, the energy involved in the sliding of a nanotube within a bundle is of the order of tenths of 1 eV, typical of van der Waals-like interactions compared to ~7 eV to break a covalent carbon bond. In addition, the shear modulus of graphite ( $G$ ) could vary anywhere from 0.2 GPa (for defective pyrolytic graphite) to 4.5 GPa (for perfect crystals). From these values, we can estimate a lower limit for the shear modulus of SWNT rope (~1 GPa),<sup>[11]</sup> and this value is in agreement with recent AFM experiments on nanotube bundles.<sup>[12]</sup> This lower limit assumes the presence of imperfections and disorder within SWNT ropes.

If the ideal shear strength between nanotubes is taken as  $G/6$  (170–750 MPa), or more realistically  $G/60$  (due to glide and stacking fault defects present in the nanotube ropes), this would correspond to 6–75 MPa for the nanotube bundles. This translates to an interfacial normal stress

in the tubes between 6.4 and 30 GPa (from the Kelly–Tyson equation<sup>[13]</sup>). Because the strength of an individual tube has been estimated to be at least 150 GPa (from a ~1 TPa elastic modulus of a perfect nanotube), it is far easier to slide a nanotube out of the bundle than to break it. Another possibility is separation of the nanotubes from the bundles by pulling normal to it. This will depend on the interfacial strength and would also cost more energy than shearing. The process can be directly connected to the elastic constants  $C_{33}$  (36.5 GPa) and  $C_{13}$  (15 GPa) of graphite (note that the surface energy connected with this layer separation is of the order of 0.2 eV/atom).

Our micro-Raman spectroscopy results also support the above hypothesis. As observed by Wood et al.,<sup>[6]</sup> placing the SWNTs in epoxy caused a  $15\text{ cm}^{-1}$  shift in the second-order  $A_{1g}$  band. This shift is due to hydrostatic compression on the tube bundles.<sup>[6]</sup> The hydrostatic compression decreases the inter-tube spacing, which will stiffen the bond between the SWNTs, thus changing the frequency of the  $D^*$ , which is sensitive to the local environment and bond length. This shift is not due to axial strain because when the composite is loaded in axial compression there is no shift in the  $D^*$  peak. This suggests that the applied stress is transformed in either buckling, bending, or twisting the nanotube network without introducing important local deformations that can be monitored by Raman. When the composite was loaded in tension there was a small shift in the peak position, as shown in Figure 3. The shift observed was about 1/10 of those observed for hydrostatic compression.<sup>[3]</sup> If the nanotubes are sliding axially within the ropes, there should be little shift in the Raman peak position as observed in compression. The slight shift in tension may be the result of a reduction in the radial stresses due to debonding, which causes an increase in the inter-tube spacing and a change in the stiffness for the out-of-plane vibrations.

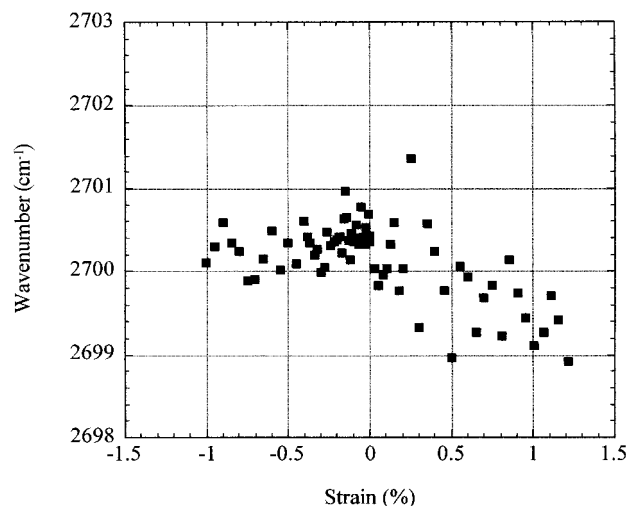


Fig. 3. Micro-Raman spectroscopy data showing the shift of the second-order  $A_{1g}$  mode for SWNTs as a function of strain applied to the nanotube-epoxy composite. It can be seen that there is no shift in compression and only a slight trend to lower wavenumbers in tension. The error bar is approximately  $\pm 0.5\text{ cm}^{-1}$ .

The nearly constant value of the Raman peak corroborates our assumption about the tube sliding within the bundle. The paper by Salvétat et al.,<sup>[12]</sup> in which SWNT bundles are loaded with an AFM, also supports this hypothesis. As the tube bundles grow in diameter, both the axial modulus and shear modulus decrease dramatically, suggesting that individual SWNTs are slipping within the bundle and decreasing the load required to deform the bundle.<sup>[12]</sup>

We stress that it is the low-modulus features of the bundles, and not the axial modulus of individual tubes, that control the mechanical stability and strength of the SWNT-polymer composite. Our experiments show strong evidence to this effect. When nanotube applications as reinforcements are considered, it is important to consider the most effective ways of obtaining strengthening: for example, by breaking bundles into individual tube fragments (say, fullerene pipes<sup>[14]</sup>) and dispersing these segments in the matrix. On the other hand, strengthening could also come from reinforcing the bundles themselves by cross-linking the tubes within bundles (e.g., via irradiation or chemical treatments) to increase the bundle rigidity and eliminate tube slippage. Even if this is achieved, one will have to worry about a strong tube-polymer interface. The formation of strong interfaces in carbon nanotube-polymer composites could be challenging but could be done through functionalization of the tube fragment ends and tube body, which then can be chemically bonded to the polymer chains.

Nanotube reinforcements, however, will increase the toughness of the composites by absorbing energy because of their highly flexible elastic behavior during loading. Other interesting applications could be in creating nanotube-filled adhesive polymer films where adhesion between nanotube-filled polymer surfaces could be greatly enhanced by some kind of reversible Velcro effect at the nanoscale, due to the attractive van der Waals forces between the nanotubes present on each of the surfaces, as was observed in Figure 1a. As we stated earlier in our work on MWNTs, the low density of the nanotubes will clearly be an advantage for composites. Nanotubes would also offer multifunctionality; for example, conducting polymer structures may be constructed at low loadings of nanotube fillers due to lower percolation thresholds needed for the high aspect ratio nanotube structures.

Received: October 20, 1999  
Final version: February 27, 2000

- [1] M. M. J. Treacy, T. W. Ebbesen, J. M. Gibson, *Nature* **1996**, *381*, 678.
- [2] N. G. Chopra, A. Zettl, *Solid State Commun.* **1998**, *105*, 297. E. W. Wong, P. E. Sheehan, C. M. Lieber, *Science* **1997**, *277*, 1971. M. R. Falvo, G. J. Clary, R. M. Taylor, V. Chi, F. P. Brooks, S. Washburn, R. Superfine, *Nature* **1997**, *389*, 582. S. Iijima, C. Brabec, A. Maiti, J. Bernholc, *J. Chem. Phys.* **1996**, *104*, 2089.
- [3] R. S. Ruoff, D. C. Lorents, *Carbon* **1995**, *33*, 925. B. I. Yakobson, C. J. Brabec, J. Bernholc, *Phys. Rev. Lett.* **1996**, *76*, 2411. M. B. Nardelli, B. I. Yakobson, J. Bernholc, *Phys. Rev. B* **1998**, *57*, 4277. C. F. Cornwell, L. T. Wille, *Solid State Commun.* **1997**, *101*, 555. J. P. Lu, *Phys. Rev. Lett.* **1997**, *79*, 1297. E. Hernández, C. Goze, P. Bernier, A. Rubio, *Phys. Rev. Lett.* **1998**, *80*, 4502. L. Vaccarini, C. Goze, L. Henrard, E. Hernández, P. Bernier, A. Rubio, unpublished.

- [4] P. Calvert, *Nature* **1999**, *399*, 210.
- [5] H. D. Wagner, O. Lourie, Y. Feldman, R. Tenne, *Appl. Phys. Lett.* **1998**, *72*, 188.
- [6] O. Lourie, H. D. Wagner, *J. Mater. Res.* **1998**, *13*, 2418.
- [7] J. R. Wood, M. D. Frogly, E. R. Meurs, A. D. Prins, T. Peijs, D. J. Dunstan, H. D. Wagner, unpublished.
- [8] L. S. Schadler, S. C. Giannaris, P. M. Ajayan, *Appl. Phys. Lett.* **1998**, *73*, 26.
- [9] M.-F. Yu, O. Lourie, M. Dyer, K. Moloni, T. F. Kelly, R. S. Ruoff, *Science* **2000**, *287*, 637.
- [10] P. M. Ajayan, O. Stephan, C. Colliex, D. Trauth, *Science* **1994**, *265*, 1212. L. Jin, C. Bower, O. Zhou, *Appl. Phys. Lett.* **1998**, *73*, 1197.
- [11] B. L. Smith, T. E. Schaffer, M. Viani, J. B. Thompson, N. A. Frederick, J. Kindt, A. Belcher, G. D. Stucky, D. E. Morse, P. K. Hansma, *Nature* **1999**, *399*, 761.
- [12] The shear modulus of an isolated SWNT is much larger and can be related to the elastic constants of graphite as  $0.5 (C_{11}-C_{12}) = 440$  GPa. This is not the magnitude relevant for the present experimental studies. In the case of the nanotube rope, its shear modulus is related to that of graphite by the ratio of the distance between tube-tube layers divided by the graphitic interplanar distance. This comes out as approximately,  $G_{\text{rope}} \sim 5 G_{\text{graphite}}$  (see [12] for details of this relationship), suggesting that for a nanotube rope (assuming disorder) the lower limit for  $G$  will be  $\sim 1$  GPa.
- [13] J. P. Salvétat, G. A. D. Briggs, J. M. Bonard, R. W. Bacsá, A. J. Kulik, T. Steckli, N. A. Burnham, L. Forro, *Phys. Rev. Lett.* **1999**, *82*, 944.
- [14] The governing equation in the Kelly-Tyson model modified for hollow tubes is:

$$\tau_{\text{NT}} = \left( \frac{\sigma_{\text{NT}}(L_c)}{2(L_c/D_{\text{NT}})} \right) \left( 1 - \frac{d_{\text{NT}}^2}{D_{\text{NT}}^2} \right) \quad (1)$$

where  $\tau_{\text{NT}}$  is the interfacial shear stress,  $\sigma_{\text{NT}}$  is the failure stress of the fiber (or nanotube or nanotube bundle),  $d_{\text{NT}}$  and  $D_{\text{NT}}$  are the inner and outer diameters of the SWNT, respectively, and  $L_c$  is the critical length of the nanotubes. This was used to calculate the normal stresses in the tubes for a critical aspect ratio of 1000, a wall thickness of 0.34 nm, and shear stresses as described in the text.

- [14] J. Liu, A. G. Rinzier, H. Dai, J. H. Hafner, R. K. Bradley, P. J. Boul, A. Lu, T. Iverson, K. Shelimov, C. B. Huffman, F. Rodriguez-Macias, Y. Shon, T. R. Lee, D. T. Colbert, R. E. Smalley, *Science* **1998**, *280*, 1253.

## Polymer-Filled Nematics: A New Class of Light-Scattering Materials for Electro-Optical Switches

By Marysia C. W. van Boxtel,\* Rob H. C. Janssen,  
Dick J. Broer,\* Hans T. A. Wilderbeek,  
Cees W. M. Bastiaansen

Over recent decades extensive research has been performed concerning the preparation and properties of two-phase mixtures based on an organic, low molecular weight liquid crystal (LC) phase and an inorganic<sup>[1-5]</sup> or polymeric phase.<sup>[6-15]</sup> For instance, electro-optical switches, based on a continuous LC phase and a dispersed phase of spherical inorganic particles with a very small diameter ( $< 20$  nm), have been investigated.<sup>[1-5]</sup> These materials switch from a

[\*] Prof. D. J. Broer,<sup>[+]</sup> M. C. W. van Boxtel, Dr. R. H. C. Janssen,<sup>[++]</sup> J. T. A. Wilderbeek, Dr. C. W. M. Bastiaansen<sup>[++]</sup>  
Eindhoven University of Technology  
Eindhoven Polymer Laboratories  
PO Box 513, NL-5600 MB Eindhoven (The Netherlands)

[+] Second address: Philips Research Laboratories, Prof. Holstlaan 4, NL-5656 AA Eindhoven, The Netherlands.

[++] Second address: ETH Zürich, Department of Materials, Institute of Polymers, Universitätstrasse 41, CH-8092 Zürich, Switzerland.